Università degli Studi di Padova

Dipartimento di Fisica e Astronomia "Galileo Galilei"

Degree in Physics

Physics Laboratory report

Timing

Author: **Luca Morselli**
Number: **1172019**

Author: **Andrea Raggio**
Number: **1178280**

Professors: **Francesco Recchia**
Luca Stevanato

Academic Year 2017-2018

Introduction

In particle detection one of the first and most important requirements is the production of a time reference for detected events. Correct definition of a particle detection time is essential to allow the production of coincidence signals between the different detectors which compose the arrays of an experimental set-up. Moreover the reduction of timing error is crucial for several measurements, such as the *Time of Flight* (TOF) technique, used to distinguish the particle type but also to measure its kinetic energy.

There are several ways to produce a timing reference for detected particles, the aim of a good technique is to increase the accuracy and reduce the dependence on particle energy (*Time walk*). The simplest one is the *Leading Edge* method, which associates the time reference of the signal with the crossing moment of a fixed threshold, for instance 0.2 as shown in Fig. 1-a. In scintillation detectors, where the rising time of the pulses is constant, this method is clearly affected by the amplitude of the signals, making it not good for the purpose. A better solution is the *Constant Fraction Discrimination* (CFD) technique (Fig. 1-b), which gives a time reference independent on pulse amplitude.

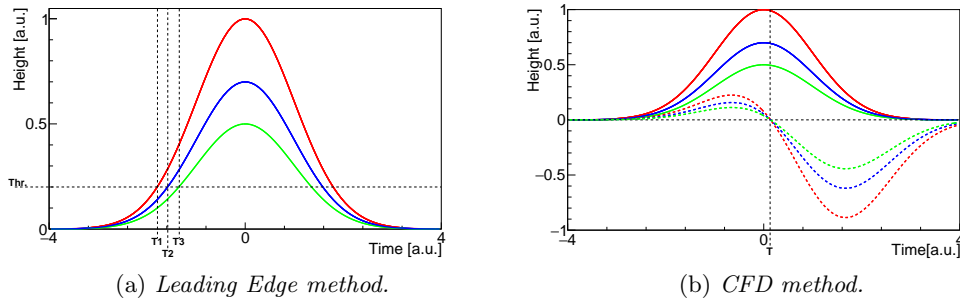

(a) *Leading Edge method.*   (b) *CFD method.*

Figure 1: *Leading Edge* (a) and *Constant Fraction Discrimination* (CFD) (b) techniques applied on three Gaussian pulses with same mean and sigma but different amplitudes. The bipolar dashed pulses in b) are generated by the CFD algorithm.

The aim of this report is to present the timing analysis performed over two scintillation detectors. Therefore the following sections will analyze these steps:

- Energy calibration of the organic scintillators and calculation of the energy resolution from the analysis of the Compton edge.

- Optimization of the external delay of the analogue CFTD to obtain the best time resolution.

- Study the time resolution behaviour as a function of the energy.

- Comparison between the timing resolutions obtained from analogue and digital treatment of the signals.

- Measurement of the speed of light.

Experimental Set Up

To perform the timing analysis two cylindrical organic scintillator EJ-228 with diameter and thickness of 5 cm were used, each one coupled with a Photonics Photomultiplier XP2020 (see Fig. 2). The anode outputs of the PMT were sent to a Quad Linear Gate FAN-IN/OUT mod. Philips 744 in order to split them. One output then was sent directly to a CAEN digitizer mod. DT5751, an ADC with a sampling rate of 1 Gs/s and a resolution of 10 bit, while the other one was sent to a Quad CFD mod. 935. The timing signals obtained from the CFD unit were processed by a CAEN Quad Logic Unit mod. N455 to produce a coincidence signal between the two detectors, used as trigger input for the digitizer. They were also to sent to an Ortec TAC unit to measure their time difference. The output of the TAC module was also digitized.
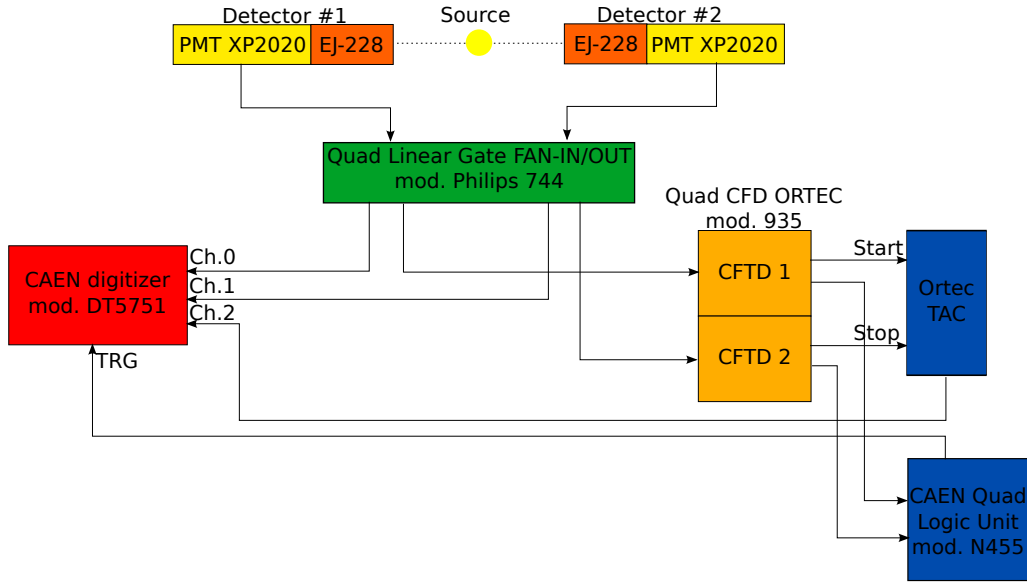

Figure 2: Experimental configuration adopted for the timing analysis.

Energy Calibration

Due to the organic composition of our detectors the photo-electric cross-section of its constituents is negligible in the energy range considered. Furthermore total absorption through multiple Compton scattering is negligible too, because of detector limited size . The detectors response will be dominated by individual Compton interaction, thus the energy spectrum is a continuous distribution that corresponds to different angles of interaction. This can be seen in the spectra acquired with the ^{22}Na source in Fig. 3.

The finite resolution of our detectors results in a shift towards lower energies depending on the detector resolution as shown in Fig. 4.

In order to obtain the energy calibration parameters, several smeared spectra were generated using the Klein-Nishina Compton Scattering cross-section (see Eq. 1) for 511 keV and 1275 keV γ respectively.

$$\frac{d\sigma}{dT} = \frac{\pi r_e^2}{m_e c^2 \alpha^2} \left(2 + \frac{s^2}{\alpha^2 (1-s)^2} + \frac{s}{1-s} \left(s - \frac{2}{\alpha} \right) \right) \tag{1}$$
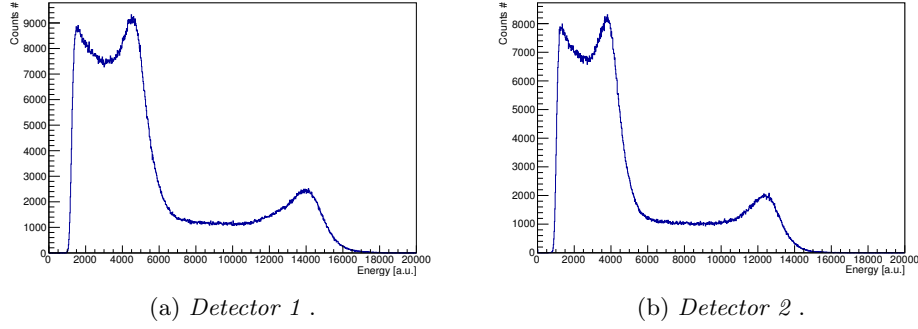
2

(a) *Detector 1* . (b) *Detector 2* .

Figure 3: *Detector 1* (a) and *Detector 2* (b) uncalibrated energy spectra obtained from a ^{22}Na γ source.
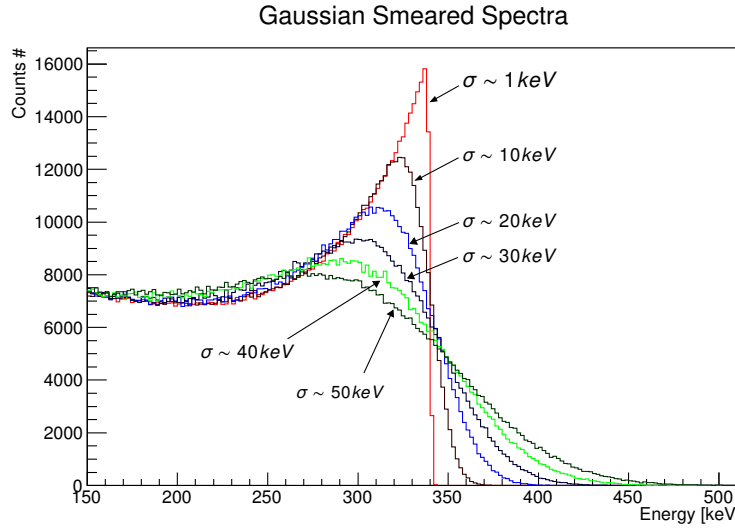

Figure 4: Gaussian smeared spectra at different σ generated using the Klein-Nishina Compton Scattering cross-section for 511 keV photons.

To locate the Compton edge then, the background from acquired spectra was removed as shown in Fig. 5. The χ^2 between experimental spectrum and Gaussian smeared spectra was minimized looping over different σ values. With the selected σ the corresponding shift of the Compton edge was computed in order to calibrate the detectors as shown in Tab. 1:

Detector	Photon Energy [keV]	σ [keV]	C.E. shifting [keV]
1	511	34	40.66
	1275	40	52.15
2	511	28	34.66
	1275	40	52.15

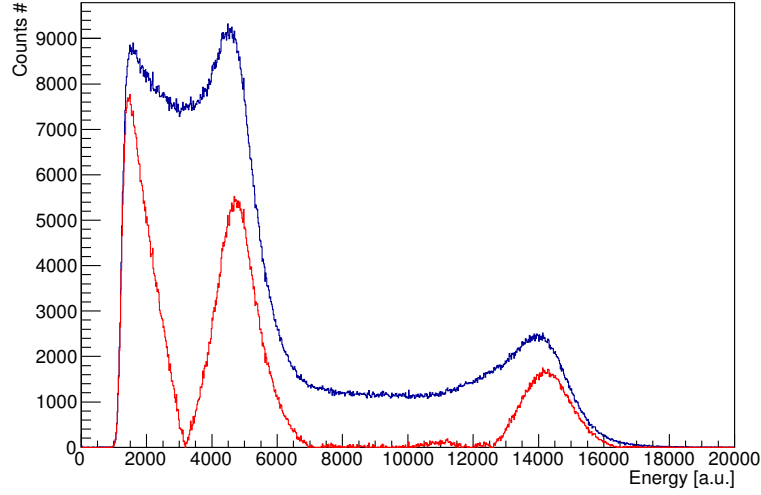Table 1: σ and C.E. shift for the two detectors.

3

Figure 5: ^{22}Na energy spectra. The blue one represent the original acquired spectrum, while the red one is obtained by background removal.
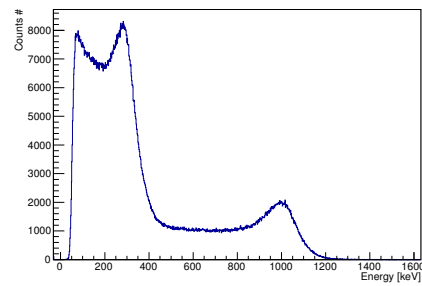
Finally the calibration parameters were computed (see Tab. 2), the ^{22}Na calibrated spectra of the two detectors are shown in Fig. 6

Detector	a [keV/channel]	b [keV]
#1	0.0748945±	-54.2511±
#2	0.083215±	-32.6856±

Table 2: Calibration parameters.
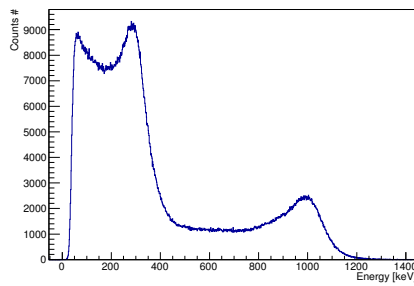
(a) *Detector 1.*

(b) *Detector 2.*

Figure 6: *Detector 1* (a) and *Detector 2* (b) energy calibrated spectra obtained from a ^{22}Na γ source.

4

TAC calibration

In order to calibrate the TAC unit, several spectra were produced using as start input the CFD timing signals and as stop the same signals delayed by a chosen value. With 2 ns delay steps the spectra of Fig. 7 was obtained, the peaks centroids were used to compute the calibration parameters performing a linear fit (see Fig. 8).
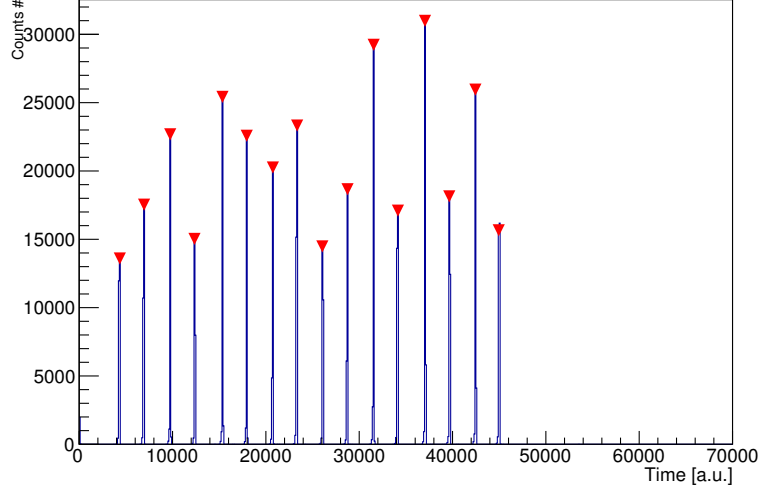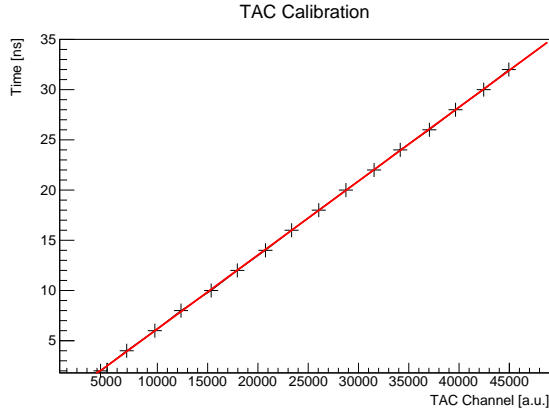

Figure 7: TAC uncalibrated spectrum obtained by an auto coincidence with 2 ns delay steps.

Figure 8: Linear fit used to compute the TAC calibration parameters.

Parameter	Value
p0	(-1.19 ± 0.04) s
p1	(7.36 ± 0.01)×10^{-4} s/ch

Fit parameters.

External delay optimization

To produce the analog timing and measure its resolution the parameters of the CFD module needed to be optimized. The thresholds were set to reject events under ≈30 keV as show in the calibrated spectra of Fig. 6, while the CFD fraction is a fixed value chosen by the producer. The delay, finally, was selected performing test measurements with values in the range 3-6 ns, using the FWHM of timing distribution as resolution indicator as shown in Fig. 9.
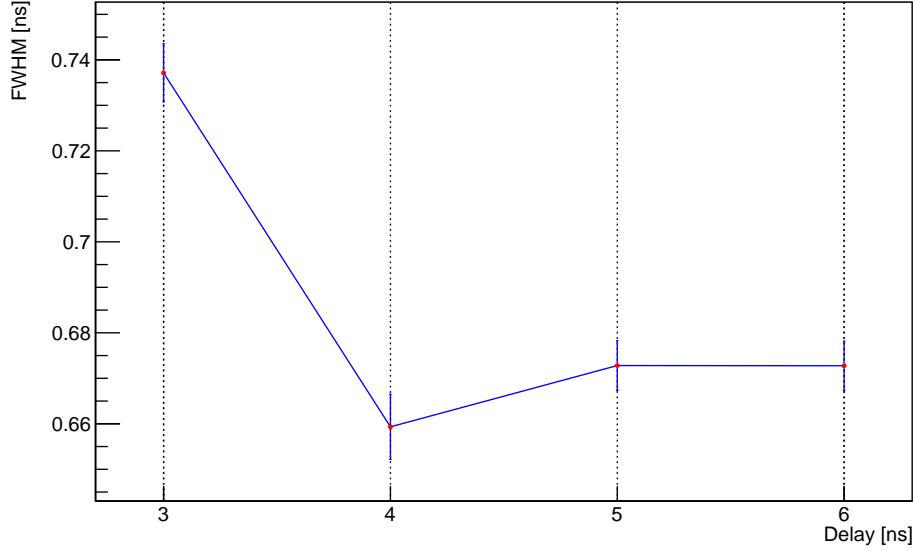

Figure 9: FWHM as a function of CFD delay.

Analog Time resolution as function of energy

In order to study the time resolution dependence as a function of energy a different radioactive source, ^{60}Co, was used. This source is chosen because of its high energy Compton Edge (≈1 MeV) that allows to study the energy dependence up to this value.

Two methods were used to characterize the timing resolution for different energies:

- Energy Windows

- Energy Thresholds

Energy Windows

The analog timing distributions were produced selecting events inside energy windows of 100 keV width in the range 100 keV-1 MeV (see Fig. 10).

For each distribution the FWHM was computed and reported in the Fig. 11 below, over the 2-D density plot of timing as function of energy.
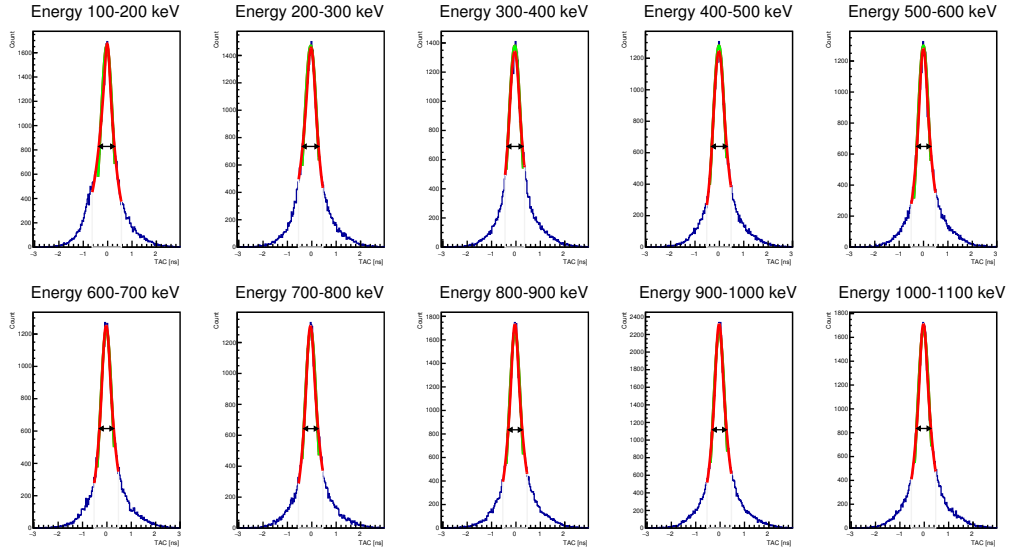
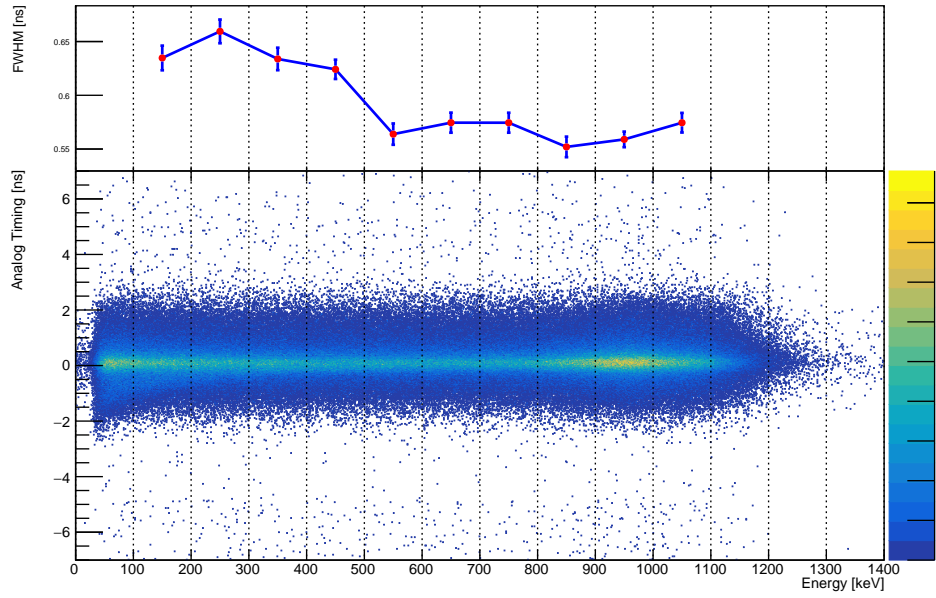Figure 10: Timing distributions obtained selecting events inside 100 keV energy windows.

Figure 11: FWHM for each energy slice over 2-D density plot of timing as function of energy.

Energy Threshold

The analog timing distributions were produced selecting events by mean of different energy thresholds from 100 keV to 1 MeV (see Fig. 12).
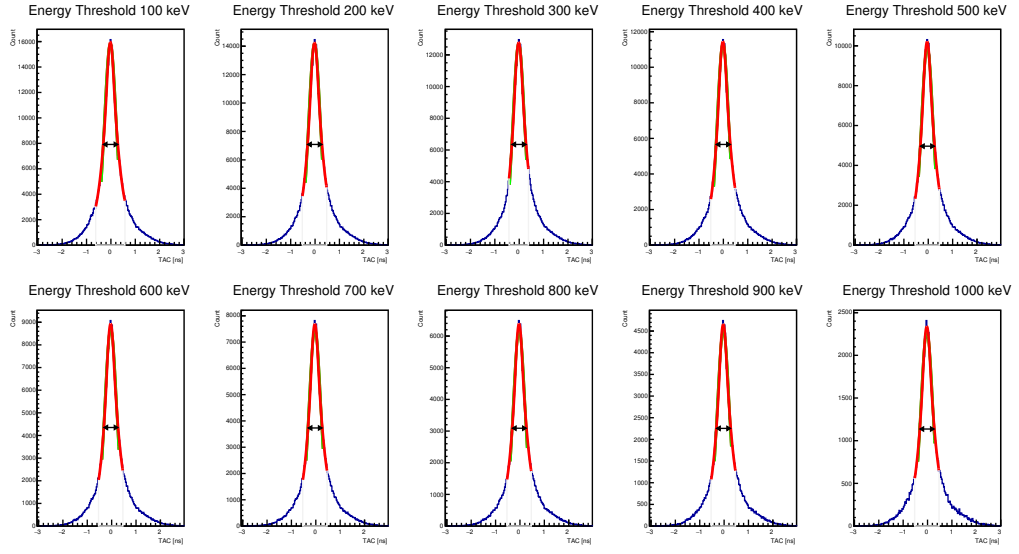
Figure 12: Timing distributions obtained selecting events inside by mean of different energy thresholds.

In the same way, for each distribution, the FWHM was computed and reported in the Fig. 13 below:
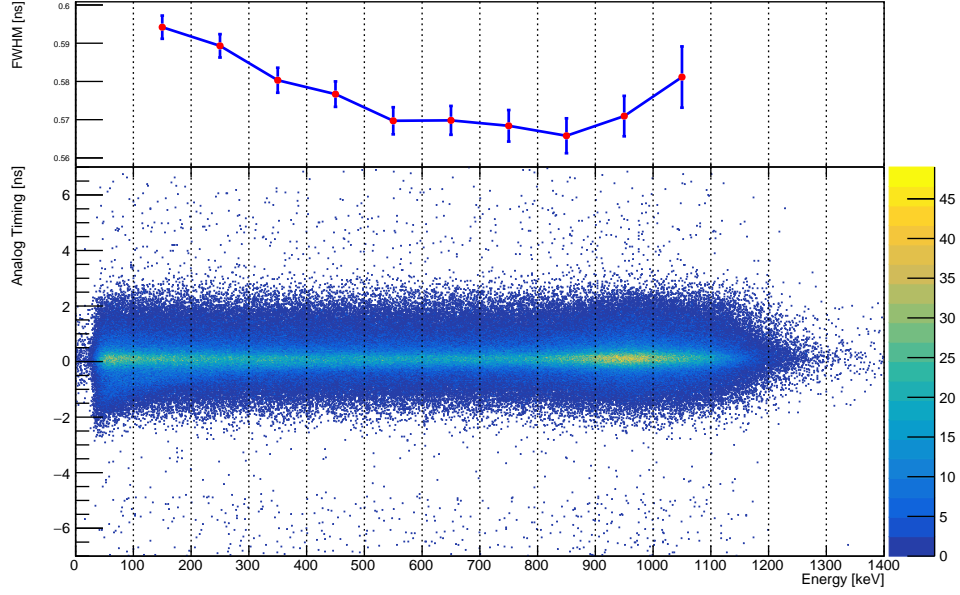

Figure 13: Lower energy threshold.

Methods comparison

The overlay of the FWHM obtained with the two methods is presented in Fig. 14. Both the curves show a minimum around the Compton edge of the spectrum, while for greater energies the increasing of FWHM could be explained by mean of multi-scattering interactions inside the detectors. The errors associated to the values, for threshold method, increase with energy. Instead for windows methods decrease moving to the Compton edge.
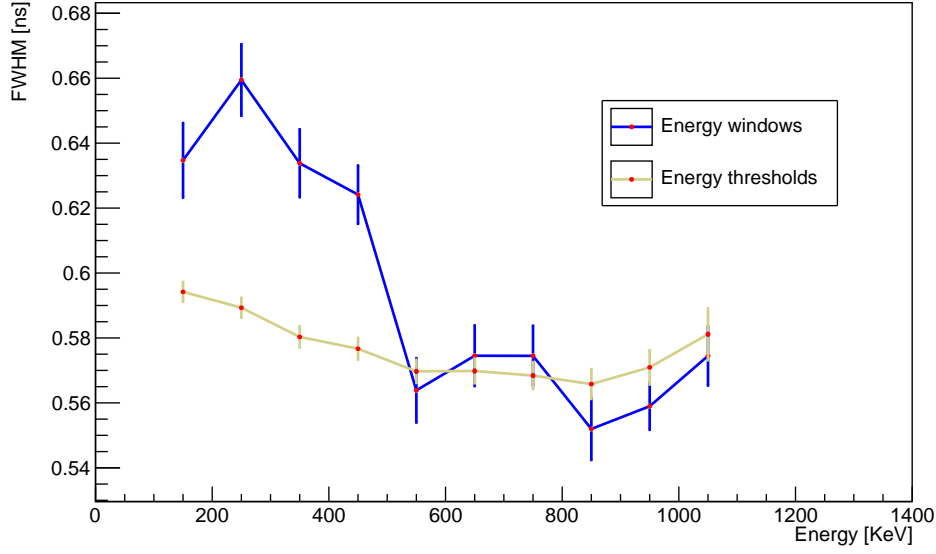
Figure 14: FWHM obtained from different energy windows and different energy thresholds compared.

Digital Timing

Digital timing algorithm uses directly the digitized waveforms, performing a digital signal treatment similar to the analog one.

The CFD method works generating a bipolar signal from the original pulse and then finding its zero crossing as time reference. Lets name W_t the digitized waveform with t an integer number (sample number). The bipolar pulse P_t is calculated as:

$$P_t = \chi W_t - W_{t-\delta}, \qquad (2)$$

where χ is a reduction fraction and δ an integer delay. Fig. shows the CFD method applied on a signal.

The intersection with the axis is found by taking the samples above and below value and interpolating to find the time reference. A cubic spline interpolation with derivative bound continuity condition up to second order was chosen. Lets consider the sample range $[t_{-1}, t_0]$ with t_0 the first sampled point after the intersection and t_{-1} the preceding one. The reconstructed pulse $f(t)$ inside the range is evaluated as follow:

$$\mathbf{f(t) = a(t - t_{-1})^3 + b(t - t_{-1})^2 + c(t - t_{-1}) + d}$$

$$\begin{cases} a = 1/18(P_{t_{-3}} - 8P_{t_{-2}} + 19P_{t_{-1}} - 19P_{t_0} + 8P_{t_1} - P_{t_2}) \\ b = 1/30(-4P_{t_{-3}} + 32P_{t_{-2}} - 58P_{t_{-1}} + 37P_{t_0} - 8P_{t_1} + P_{t_2}) \\ c = 1/90(7P_{t_{-3}} - 56P_{t_{-2}} - 11P_{t_{-1}} + 74P_{t_0} - 16P_{t_1} + 2P_{t_2}) \\ d = P_{t_{-1}} \end{cases}$$

We can perform a digital timing that reconstructs all the analog chain using software. In order to do so we need the signal waveforms provided by the DT5751

CAEN digitizer[1]. The digitized waveform then is manipulated in order to obtain a bipolar signal (Fig.15). Then troughtout an algorithms we have to find the zero
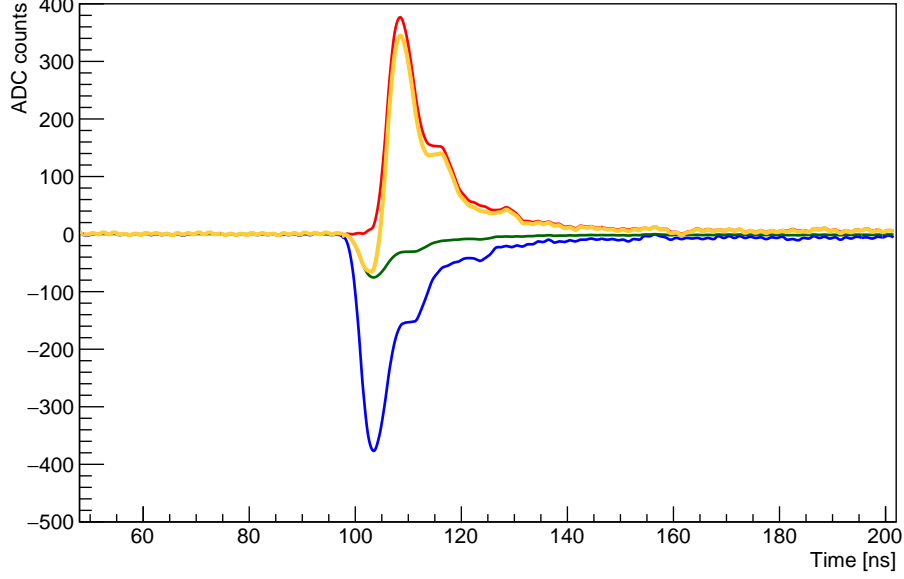

Figure 15: Digital waveforms manipulations used to get the bipolar signal

of the signal that is the time that we associate to the event.

descrizione dell'algoritmo e del fit c2 etc etc

The bipolar signal shape depends on two parameter that we need to tune in order to optimize the time resolution:

- Fraction

- Delay

Speed of light

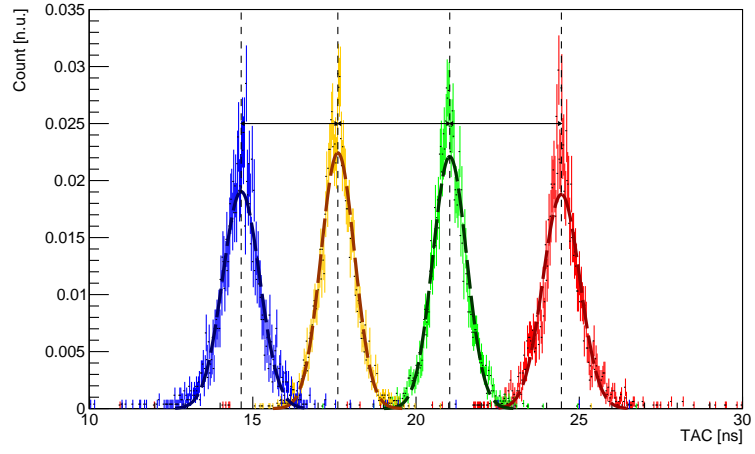$$T_1 = \frac{X+}{den} \tag{3}$$

---

[1]with a sampling rate of 1 GS/s
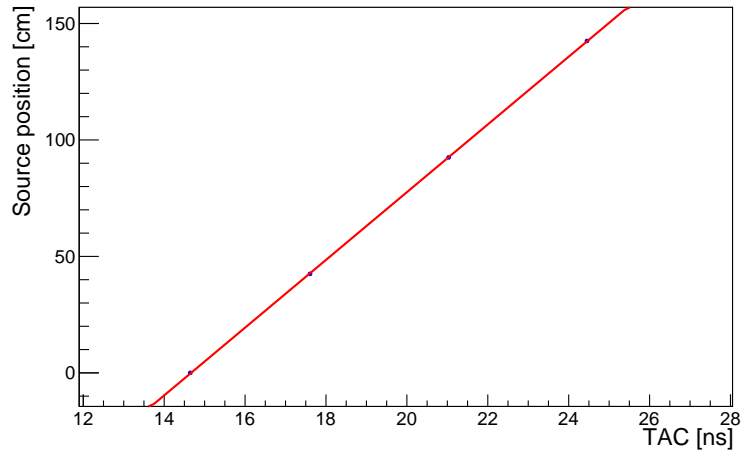
Figure 16: TAC distribution in the four different positions.

Figure 17: Position vs Time (the angular coefficient is c/2).

12